Series of topological phase transitions in TiTe$_2$ under strain

Qingyun Zhang, Yingchun Cheng, and Udo Schwingenschlögl[*]

PSE Division, King Abdullah University of Science and Technology, Thuwal 23955-6900, Kingdom of Saudi Arabia

First-principles calculations are performed to investigate the topological properties of TiTe$_2$ under hydrostatic pressure, uniaxial strain, and biaxial strain. It is found that the system is unusually accessible to strain effects and the first compound that under hydrostatic pressure (up to experimentally reasonable 30 GPa) is subject to a series of four topological phase transitions, which are related to band inversions at different points of the Brillouin zone. Therefore, TiTe$_2$ enables experimental access to all these transitions in a single compound.

As a new kind of quantum matter, topological insulators (TIs) have been intensively studied during the last decade.[1–4] They are characterized by a band gap in the bulk and an odd number of gapless edge/surface states. The surface states originate from spin-orbit coupling and are topologically protected by time-reversal symmetry, which makes TIs promising materials for spintronics and quantum computation applications. Many three-dimensional (3D) TIs have been theoretically predicted and experimentally confirmed.[5–13] However, the search for TIs that are more suitable for experimental investigations and applications is still a key issue. In this context, strain engineering has proven to be a fruitful path, as HgTe had been predicted to be a strong TI under strain.[2] Various attempts subsequently have been directed to the investigation of strain-induced topological phase transitions.[14–22] Specifically, the properties at the transition point between the topological and trivial phases, such as sharp Raman anomalies[23] and Weyl semimetallic phases with broken symmetry,[24,25] have attracted attention, because the phase transitions are essential for understanding the underlying physics.

Based on density functional theory, several methods have been introduced for discovering 3D TIs,[8] particularly the investigation of the surface electronic structure, the adiabatic continuity band transformation, the band inversion picture, and the direct calculation of the $\mathbb{Z}_2$ topological invariants. The latter have been introduced by Kane and Mele to characterize time-reversal symmetry protected systems.[1] Values of $\mathbb{Z}_2 = 0$ and 1 represent topologically trivial and nontrivial phases, respectively. In a 3D system, the four $\mathbb{Z}_2$ topological invariants $(\nu_0; \nu_1 \nu_2 \nu_3)$ are used for classification. A nonzero ν_0 indicates that the system is a strong TI, whereas when $\nu_0 = 0$ the system has to be further classified according to ν_1, ν_2, and ν_3. Systems with $\nu_{1/2/3} \neq 0$ are called weak TIs, while (0;000) is a normal insulator. A strong TI cannot be directly connected to a weak TI or a normal insulator by any adiabatically continuous transformation of the band structure.

TiTe$_2$ is isostructural to the compound 1T-TiSe$_2$, which has been investigated for decades because of its charge density wave.[26,27] Under pressure 1T-TiSe$_2$ transforms from a charge density wave into a superconducting phase at low temperature,[28] indicating that further interesting effects can be expected in titanium chalcogenides under strain. In the present paper we therefore study by density functional theory the topological properties of TiTe$_2$, which turn out to be surprisingly rich. In particular, we show that hydrostatic pressure drives a series of transitions between topological and trivial phases related to band inversions at different points of the Brillouin zone, enabling experiment to access them all in a single compound at reasonable pressure.

The calculations are carried out using the QUANTUM ESPRESSO code[29] with norm-conserving pseudopotentials and the generalized gradient approximation in the Perdew-Burke-Ernzerhof scheme. A kinetic energy cutoff of 680 eV is employed for the wave functions together with a $12 \times 12 \times 10$ k mesh. Bulk TiTe$_2$ has a layered hexagonal structure with space group $P\bar{3}m1$ (No. 164). There are three atoms in the unit cell, with the Ti and Te atoms located at $1a$ $(0, 0, 0)$ and $2d$ $(1/3, 2/3, \bar{z})$ Wyckoff sites, respectively. The unit cell and Brillouin zone of TiTe$_2$ are shown in Fig. 1. Despite the strong ionic-covalent bonding within each triple-layer slab, adjacent slabs are weakly coupled by van der Waals forces. We study hydrostatic pressure as well as uniaxial and biaxial strain, which does not alter the symmetry of the system. The uniaxial strain is applied along the [001] direction and the biaxial strain within the xy plane. The magnitude of the uniaxial strain is defined as $\epsilon_{[001]} \equiv \frac{c - c_0}{c_0} \times 100\%$ and that of the biaxial strain as $\epsilon_{xy} \equiv \frac{a - a_0}{a_0} \times 100\%$, where a_0 and c_0 are the in-plane and out-of-plane equilibrium lattice constants.

To characterize topological insulators parity analyses are widely adopted and work well for centrosymmetric systems, as only knowledge about the Bloch functions at the time-reversal invariant momenta (TRIM) of the Brillouin zone is required. In a 3D system there are eight TRIM: $\Gamma_{(n_1,n_2,n_3)} = 1/2(n_1 b_1 + n_2 b_2 + n_3 b_3)$, where $b_{1/2/3}$ are the primitive reciprocal lattice vectors with $n_{1/2/3} = 0$ or 1. The topological invariant then is given by the product of the parity eigenvalues at the eight TRIM. Recently, two other approaches have been proposed for calculating the $\mathbb{Z}_2$ invariants, which work in both centrosymmetric and noncentrosymmetric systems. One is the Berry connection and Berry curvature integration over half of the Brillouin zone[30] and the other is the evolution of the Wannier function centers (WFCs) during a time-reversal pumping process.[31,32] Here, we employ the second method to confirm the results of the parity analysis. The required calculation steps are briefly introduced as follows. First, one has to calculate the overlap matrix

$$F(k_1,k_2)_{mn} = \langle m,k_1,k_2 \mid n,k_1 + \Delta k_1,k_2 \rangle, \qquad (1)$$

where $|n,k_1,k_2\rangle$ represents the nth occupied band and $\Delta k_1 = 2\pi/(M \cdot a)$ is the discrete spacing of M points. From this
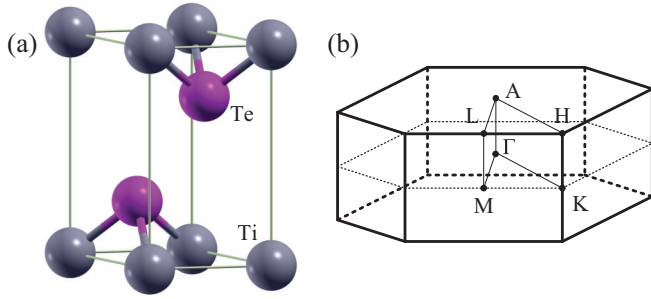
FIG. 1. (Color online) (a) Unit cell of TiTe$_2$ and (b) corresponding Brillouin zone.

matrix, the unitary $2N \times 2N$ ($2N$ is the number of occupied bands) square matrix

$$D(k_2) = \prod_{j=0}^{M} F(j \cdot \Delta k_1, k_2) \qquad (2)$$

is obtained, with the complex eigenvalues

$$\lambda_\ell(k_2) = |\lambda_\ell(k_2)| e^{i\theta_\ell(k_2)}, \quad \ell = 1,2,\ldots,2N. \qquad (3)$$

The WFC, represented by θ_ℓ, will evolve with k_2 during a time-reversal pumping process. The topological invariant is then calculated by the number of crossings of any horizontal ($\theta = $ constant) reference line with the evolution curves of the WFC, modulo 2. In a 3D system it is necessary to calculate two invariants, z_0 and z_π, in different planes, $k_3 = 0$ and $k_3 = \pi$, to obtain $\nu_0 \equiv (z_0 - z_\pi) \bmod 2$. As an example, the system is topologically nontrivial when the evolution curves of the WFC cross an arbitrary reference line an odd number of times in the $k_3 = 0$ plane ($z_0 = 1$) and an even number of times in the $k_3 = \pi$ plane ($z_\pi = 0$) or vice versa. On the other hand, when the evolution curves cross the reference line an even ($z_0 = z_\pi = 0$)

or odd ($z_0 = z_\pi = 1$) number of times in both the $k_3 = 0$ and $k_3 = \pi$ planes the system is topologically trivial.

We have performed a structure relaxation using the experimental lattice constants as input parameters and neglecting the spin-orbit coupling. The converged lattice constants a_0 and c_0 are 3.81 Å and 6.92 Å, and thus close to the experimental values ($a_0 = 3.78$ Å, $c_0 = 6.50$ Å).[33,34] The $\bar{z}$ value of the relaxed structure, which characterizes the relative atomic position, is 0.253. The electronic band structure without strain, as shown in Fig. 2(a), indicates that bulk TiTe$_2$ is a semimetal, which agrees with previous calculations.[33] The valence band maximum is located at the Γ point, while the conduction band minimum is located at the L point. The conduction and valence bands are separated by a band gap throughout the Brillouin zone, where the states around the Fermi level are mostly contributed by the Te p and Ti d orbitals. To identify the variation of the orbital occupations under strain, we project the bands onto the Te p and Ti d orbitals, as indicated by the colors in Fig. 2. Five conduction bands are dominated by the Ti d orbitals, whereas six valence bands are dominated by the Te p orbitals. Moreover, there is weak p-d hybridization as a result of the lower electronegativity of the Te atoms.

Due to the inversion symmetry of TiTe$_2$, we can apply the parity analysis. The eight TRIM are 1Γ, 3M, 1A, and 3L, as illustrated in Fig. 1(b). By checking the parities of the valence states at the eight TRIM, we find that the topological invariants of TiTe$_2$ without strain are (0;000), which means that we have a trivial semimetal. Band structures for 3, 8, and 15 GPa pressure are given in Figs. 2(b)–2(d). With increasing pressure the lattice parameter decreases and the interaction between the atomic orbitals becomes stronger, making the band structure more dispersive. For 3 GPa pressure, as compared to the situation without strain, one of the valence bands changes from Te p to Ti d domination at the A point, which signifies that a band inversion has occurred. Higher pressure leads to
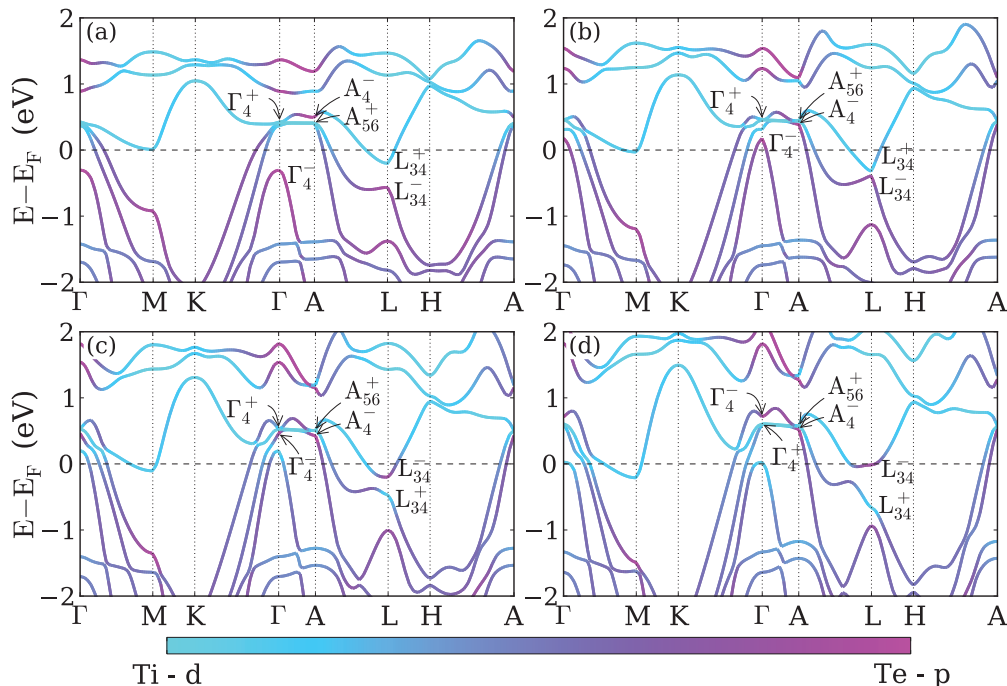
FIG. 2. (Color online) Band structures of TiTe$_2$ without (a) and with (b) 3 GPa, (c) 8 GPa, and (d) 15 GPa hydrostatic pressure.
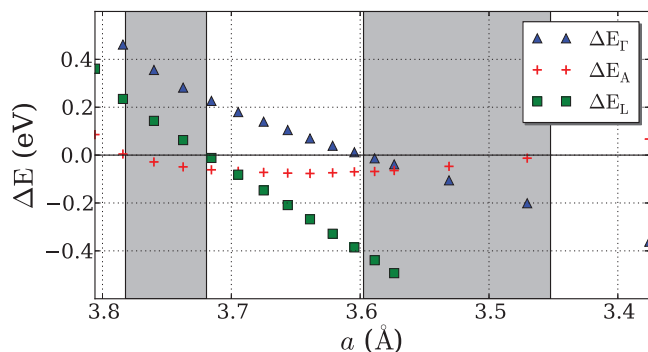
FIG. 3. (Color online) Energy difference between states around the Fermi level: variation with the lattice parameter.

a band inversion at the L point, which is shown for 8 GPa in Fig. 2(c). The band structure under 15 GPa pressure is depicted in Fig. 2(d). As compared to Fig. 2(c), a band inversion occurs at the Γ point, while the band order around the Fermi energy at the other TRIM is not changed. Since the symmetry of the system is not affected by the hydrostatic pressure, we still can apply the parity analysis. It is found that the topological invariants under 3, 8, and 15 GPa hydrostatic pressure are (1;001), (0;000), and (1;001), respectively. Based on these results, the system undergoes a series of topological phase transitions under hydrostatic pressure.

For increasing pressure from 0 to 30 GPa, band inversions occur consecutively at the A, L, Γ, and A points. Figure 3 illustrates the variation of the energy differences $\Delta E_\Gamma = E(\Gamma_4^+) - E(\Gamma_4^-)$, $\Delta E_A = E(A_4^-) - E(A_{56}^+)$, and $\Delta E_L = E(L_{34}^+) - E(L_{34}^-)$ with the lattice parameter. The $+/-$ sign represents even/odd parity. Interpolating the data,

we can predict that the phase transitions occur at the critical points $a = 3.78$ Å, 3.72 Å, 3.60 Å, and 3.45 Å, where ΔE_Γ, ΔE_A, or ΔE_L cross zero. The regions in which the system is in topological and trivial phases are indicated by dark and light backgrounds. The results suggest that the topological property changes several times as a function of the lattice parameter.

Band structures for uniaxial compressive (-5%), uniaxial tensile ($+5\%$), biaxial compressive (-2%), and biaxial tensile ($+2\%$) strain are depicted in Figs. 4(a)–4(d). We notice that the band structure under uniaxial compressive strain is similar to that under biaxial tensile strain, see Figs. 4(a) and 4(d), which can be attributed to the fact that both kinds of strain lead to the same deformation of the unit cell: a shrinkage along the [001] direction and an expansion within the xy plane. A similarity is also observed between the band structures for uniaxial tensile and biaxial compressive strain, see Figs. 4(b) and 4(c). In Fig. 4(a) we find no band inversion at the eight TRIM as compared to the case without strain, although the band order changes at the M point. In contrast, in Fig. 4(b) the A_{56}^- band shifts above the A_4^- band. Moreover, in Fig. 4(c) a band inversion occurs at the A point, similar to Fig. 4(b), while in Fig. 4(d) the band order is the same as without strain. By applying the parity analysis, the topological invariants are computed to be (1;001) for -5% uniaxial and $+2\%$ biaxial strain and (0;000) for $+5\%$ uniaxial and -2% biaxial strain.

Although TiTe$_2$ is a semimetal it is still of interest to compute the evolution of the WFC based on valence bands[32] and to compare with the parity eigenvalue method. We have to calculate the WFC in two of the six Brillouin zone planes to obtain the topological invariant of the system. Without strain the evolution along the k_2 direction in the $k_3 = 0$ and $k_3 = \pi$ planes is illustrated in Figs. 5(a) and 5(b). By the dashed reference line, we find that both evolution curves cross
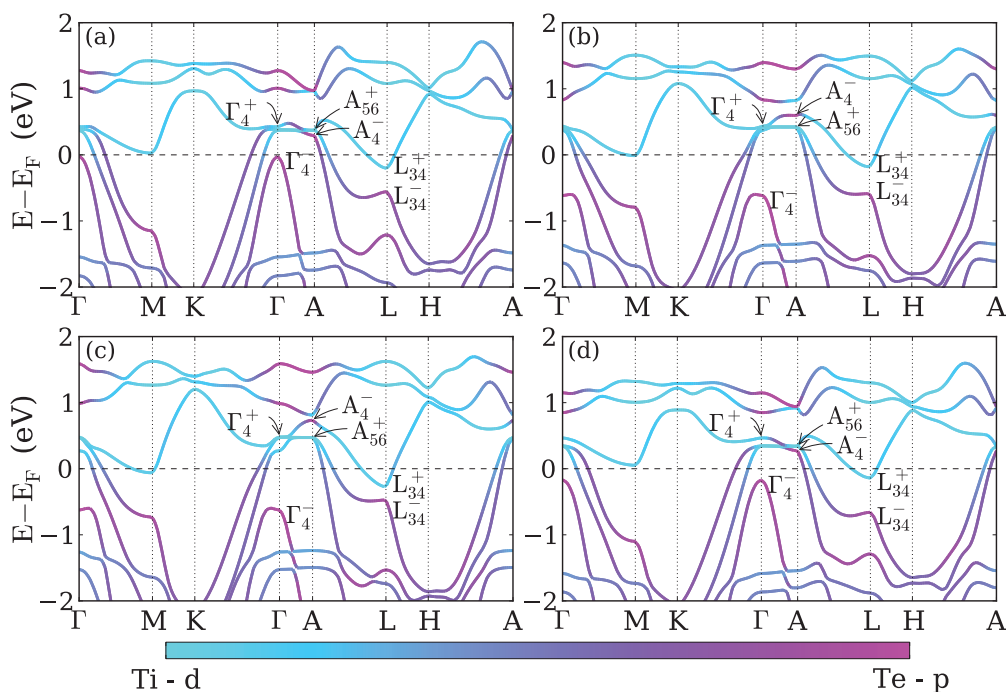
FIG. 4. (Color online) Band structures of TiTe$_2$ under (a) uniaxial compressive (-5%), (b) uniaxial tensile ($+5\%$), (c) biaxial compressive (-2%), and (d) biaxial tensile ($+2\%$) strain.
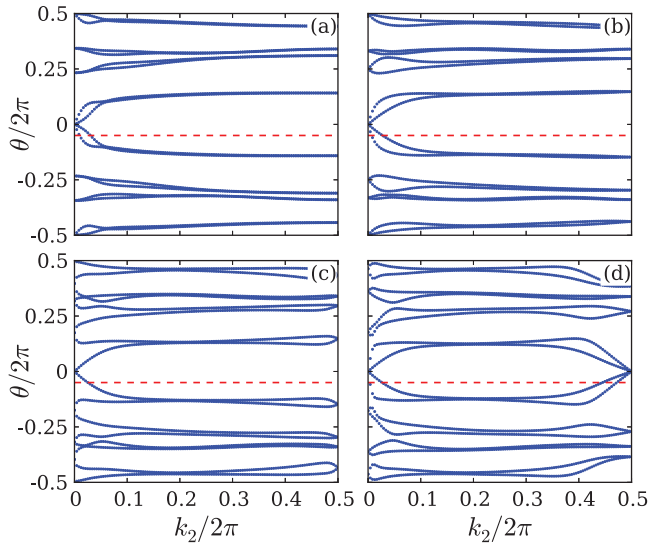
FIG. 5. (Color online) Evolution curves of the WFC in the (a) $k_3 = 0$ plane, (b) $k_3 = \pi$ plane without strain, (c) $k_3 = \pi$ plane with 3 GPa pressure, and (d) $k_3 = \pi$ plane with 8 GPa pressure.

FIG. 6. (Color online) Evolution curves of the WFC in the $k_3 = \pi$ plane with (a) uniaxial compressive (-5%), (b) uniaxial tensile ($+5\%$), (c) biaxial compressive (-2%), and (d) biaxial tensile ($+2\%$) strain.

two (even) times, resulting in $z_0 = z_\pi = 0$. The topological invariant equals $\nu_0 \equiv (z_0 - z_\pi) \bmod 2 = 0$, which means that the system is in a trivial phase. For 3 and 8 GPa pressure the evolutions in the $k_3 = 0$ plane give the same result $z_0 = 0$, while the $k_3 = \pi$ plane is addressed in Figs. 5(c) and 5(d). For 3 GPa pressure the Kramers pairs switch partners at the end of the time-reversal pumping process. Because the evolution curves cross the reference line one (odd) time and the topological invariant ν_0 amounts to 1, the system is in a topological phase. In contrast, for 8 GPa pressure the Kramers pairs do not switch partners, leading to a trivial phase. We further calculate the evolution of the WFC for 15 GPa pressure, obtaining $z_0 = 1$ and $z_\pi = 0$. The Kramers pairs switch partners in the $k_3 = 0$ plane due to the fact that band inversion occurs at the Γ point and not at the A and L points between 8 to 15 GPa. All these results are in agreement with the parity analysis.

Under uniaxial and biaxial strain, band inversions occur at the A and L points. The topological invariant in the $k_3 = 0$ plane is calculated to be $z_0 = 0$ for both $\pm5\%$ uniaxial strain and $\pm2\%$ biaxial strain. The evolution of the WFC in the $k_3 = \pi$ plane is shown in Figs. 6(a)–6(d). For uniaxial compressive and biaxial tensile strain the Kramers pairs switch partners, see Figs. 6(a) and 6(d), which reflects a topological phase, while for uniaxial tensile and biaxial compressive strain, see Figs. 6(b) and 6(c), the Kramers pairs do not switch partners and we have a trivial phase. These results also agree with the parity analysis.

In conclusion, we have studied the band structures and topological invariants of TiTe$_2$ under different types of strain, employing density functional theory within the generalized gradient approximation. The topological invariants are calculated by parity analysis, which is possible because of the inversion symmetry of the compound, and then confirmed by the evolution of the WFC. For comparison, we have repeated the calculations using the local density approximation, for which smaller lattice parameters are obtained. Since the topological property is very sensitive to the lattice parameter according to our results for the generalized gradient approximation, the employed approximation thus can be critical. However, we have confirmed that our conclusions concerning strain-induced topological phase transitions remain valid. Our results demonstrate that TiTe$_2$ undergoes topological phase transitions for increasing uniaxial and biaxial strain and, importantly, a full series of transitions under hydrostatic pressure. A similarly strong dependence of the electronic structure on strain for other compounds is a topic for future research. In contrast to spin-orbit coupling, which is an intrinsic property of a material, strain is externally applied and thus can be controlled to tune the band inversion. This enables insight into the physics of topological phase transitions by Raman spectroscopy.[23] By its rich topological phase diagram under hydrostatic pressure, TiTe$_2$ therefore is an ideal candidate for experimental studies.

*Udo.Schwingenschlogl@kaust.edu.sa

[1]C. L. Kane and E. J. Mele, Phys. Rev. Lett. **95**, 146802 (2005).
[2]L. Fu and C. L. Kane, Phys. Rev. B **76**, 045302 (2007).
[3]M. Z. Hasan and C. L. Kane, Rev. Mod. Phys. **82**, 3045 (2010).
[4]X.-L. Qi and S.-C. Zhang, Rev. Mod. Phys. **83**, 1057 (2011).
[5]H.-J. Zhang, C.-X. Liu, X.-L. Qi, X. Dai, Z. Fang, and S.-C. Zhang, Nature Phys. **5**, 438 (2009).
[6]B. A. Bernevig, T. L. Hughes, and S.-C. Zhang, Science **314**, 1757 (2006).
[7]B. H. Yan and S.-C. Zhang, Rep. Prog. Phys. **75**, 096501 (2012).

[8] W. X. Feng and Y. G. Yao, Sci. China Phys. Mech. Astron. **55**, 2199 (2012).

[9] X. Dai, T. L. Hughes, X. L. Qi, Z. Fang, and S. C. Zhang, Phys. Rev. B **77**, 125319 (2008).

[10] Y. Xia, D. Qian, D. Hsieh, L. Wray, A. Pal, H. Lin, A. Bansil, D. Grauer, Y. S. Hor, R. J. Cava, and M. Z. Hasan, Nature Phys. **5**, 398 (2009).

[11] Y. L. Chen, J. G. Analytis, J.-H. Chu, Z. K. Liu, S.-K. Mo, X. L. Qi, H. J. Zhang, D. H. Lu, X. Dai, Z. Fang, S. C. Zhang, I. R. Fisher, Z. Hussain, and Z.-X. Shen, Science **325**, 178 (2009).

[12] D. Hsieh, Y. Xia, D. Qian, L. Wray, F. Meier, J. H. Dil, J. Osterwalder, L. Patthey, A. V. Fedorov, H. Lin, A. Bansil, D. Grauer, Y. S. Hor, R. J. Cava, and M. Z. Hasan, Phys. Rev. Lett. **103**, 146401 (2009).

[13] D. Hsieh, Y. Xia, D. Qian, L. Wray, J. H. Dil, F. Meier, J. Osterwalder, L. Patthey, J. G. Checkelsky, N. P. Ong, A. V. Fedorov, H. Lin, A. Bansil, D. Grauer, Y. S. Hor, R. J. Cava, and M. Z. Hasan, Nature (London) **460**, 1101 (2009).

[14] W. Feng, W. Zhu, H. H. Weitering, G. M. Stocks, Y. Yao, and D. Xiao, Phys. Rev. B **85**, 195114 (2012).

[15] L. Winterfeld, L. A. Agapito, J. Li, N. Kioussis, P. Blaha, and Y. P. Chen, Phys. Rev. B **87**, 075143 (2013).

[16] L. A. Agapito, N. Kioussis, W. A. Goddard III, and N. P. Ong, Phys. Rev. Lett. **110**, 176401 (2013).

[17] M. S. Bahramy, B.-J. Yang, R. Arita, and N. Nagaosa, Nature Commun. **3**, 679 (2012).

[18] Z. Zhu, Y. Cheng, and U. Schwingenschlögl, Phys. Rev. Lett. **108**, 266805 (2012).

[19] Y. Sun, X. Q. Chen, C. Franchini, D. Li, S. Yunoki, Y. Li, and Z. Fang, Phys. Rev. B **84**, 165127 (2011).

[20] Y. Sun, X. Q. Chen, S. Yunoki, D. Z. Li, and Y. Li, Phys. Rev. Lett. **105**, 216406 (2010).

[21] S. M. Young, S. Chowdhury, E. J. Walter, E. J. Mele, C. L. Kane, and A. M. Rappe, Phys. Rev. B **84**, 085106 (2011).

[22] B. Sa, J. Zhou, Z. Song, Z. Sun, and R. Ahuja, Phys. Rev. B **84**, 085130 (2011).

[23] A. Bera, K. Pal, D. V. S. Muthu, S. Sen, P. Guptasarma, U. V. Waghmare, and A. K. Sood, Phys. Rev. Lett. **110**, 107401 (2013).

[24] Z. Wang, Y. Sun, X. Q. Chen, C. Franchini, G. Xu, H. Weng, X. Dai, and Z. Fang, Phys. Rev. B **85**, 195320 (2012).

[25] V. Pardo, J. C. Smith, and W. E. Pickett, Phys. Rev. B **85**, 214531 (2012).

[26] M. Calandra and F. Mauri, Phys. Rev. Lett. **106**, 196406 (2011).

[27] Z. Y. Zhu, Y. C. Cheng, and U. Schwingenschlögl, Phys. Rev. B **85**, 245133 (2012).

[28] A. F. Kusmartseva, B. Sipos, H. Berger, L. Forró, and E. Tutiš, Phys. Rev. Lett. **103**, 236401 (2009).

[29] P. Giannozzi, S. Baroni, N. Bonini, M. Calandra, R. Car, C. Cavazzoni, D. Ceresoli, G. L. Chiarotti, M. Cococcioni, I. Dabo, A. D. Corso, S. de Gironcoli, S. Fabris, G. Fratesi, R. Gebauer, U. Gerstmann, C. Gougoussis, A. Kokalj, M. Lazzeri, L. Martin-Samos, N. Marzari, F. Mauri, R. Mazzarello, S. Paolini, A. Pasquarello, L. Paulatto, C. Sbraccia, S. Scandolo, G. Sclauzero, A. P. Seitsonen, A. Smogunov, P. Umari, and R. M. Wentzcovitch, J. Phys.: Condens. Matter **21**, 395502 (2009).

[30] T. Fukui and Y. Hatsugai, J. Phys. Soc. Jpn. **76**, 053702 (2007).

[31] R. Yu, X. L. Qi, A. Bernevig, Z. Fang, and X. Dai, Phys. Rev. B **84**, 075119 (2011).

[32] A. A. Soluyanov and D. Vanderbilt, Phys. Rev. B **83**, 235401 (2011).

[33] Z. Y. Zhu, Y. C. Cheng, and U. Schwingenschlögl, Phys. Rev. Lett. **110**, 077202 (2013).

[34] Y. Arnaud and M. Chevreton, J. Solid State Chem. **39**, 230 (1981).